UCLA
UCLA Previously Published Works

Title
Eddy-mediated transport of warm Circumpolar Deep Water across the Antarctic Shelf Break

Permalink
https://escholarship.org/uc/item/1m25w146

Journal
Geophysical Research Letters, 42(2)

ISSN
0094-8276

Authors
Stewart, AL
Thompson, AF

Publication Date
2015-01-28

DOI
10.1002/2014GL062281

Peer reviewed

Eddy-mediated transport of warm Circumpolar Deep Water across the Antarctic Shelf Break

Andrew L. Stewart,[1] and Andrew F. Thompson[2]

The Antarctic Slope Front (ASF) modulates ventilation of the abyssal ocean via the export of dense Antarctic Bottom Water (AABW), and constrains shoreward transport of warm Circumpolar Deep Water toward marine-terminating glaciers. Along certain stretches of the continental shelf, particularly where AABW is exported, density surfaces connect the shelf waters to the mid-depth CDW offshore, offering a pathway for mesoscale eddies to transport CDW directly onto the continental shelf. Using an eddy-resolving process model of the ASF, the authors show that mesoscale eddies can supply a dynamically significant transport of heat and mass across the continental shelf break. The shoreward transport of surface waters is purely wind-driven, whilst the shoreward CDW transport is entirely due to mesoscale eddy transfer. The CDW flux is sensitive to all aspects of the model's surface forcing and geometry, suggesting that shoreward eddy heat transport may be localized to favorable sections of the continental slope.

1. Introduction

The Antarctic continental shelf is almost completely encircled by the Antarctic Slope Front [ASF, *Jacobs*, 1991]. The exchange of water masses across the ASF is critical to the global ocean circulation and the stability of the Antarctic ice sheet. Antarctic Bottom Water (AABW) exported from the continental shelves of the Weddell and Ross Seas supplies the deepest branch of the global overturning circulation [*Orsi et al.*, 1999; *Lumpkin and Speer*, 2007]. AABW fills around 50% of the sub-surface ocean [*Gebbie and Huybers*, 2011], "ventilating" the abyssal ocean with relatively oxygen-rich waters [*Orsi et al.*, 2001]. This abyssal circulation stores around 30 times as much carbon as the atmosphere, so small changes in AABW export could substantially alter the atmospheric/oceanic partitioning of CO_2 [*Skinner et al.*, 2010]. Meanwhile the transport of relatively warm Circumpolar Deep Water (CDW) onto the continental shelf supplies the heat needed to maintain coastal polynyas and melt the bases of the Antarctic ice shelves [*Nicholls et al.*, 2009; *Hattermann et al.*, 2014]. In the Bellingshausen and Amundsen Seas there is no distinguishable ASF, and CDW floods the local ice shelf cavities. The observed retreat of the region's marine-terminating glaciers has been attributed to changes in the thickness of this CDW layer [*Jacobs et al.*, 2011; *Schmidtko et al.*, 2014].

---

[1]Department of Atmospheric and Oceanic Sciences, University of California, Los Angeles, Los Angeles, California, USA.

[2]Environmental Sciences and Engineering, California Institute of Technology, Pasadena, California, USA.

Several recent studies have highlighted that mesoscale eddies could make an important contribution to exchanges across the Antarctic shelf break. For example, *Nøst et al.* [2011] and *Hattermann et al.* [2014] showed that eddies carry CDW across the shelf break and beneath Fimbul ice shelf. *St-Laurent et al.* [2013] showed that the presence of a coastal trough in the Bellingshausen Sea continental shelf can enhance the heat transport to the adjacent ice shelves by accumulating warm anticyclonic eddies from offshore. *Nakayama et al.* [2014] showed that eddies carry newly-formed AABW across the continental slope from a coastal polynya off Cape Darnley, in East Antarctica. In a more general configuration *Stewart and Thompson* [2012, 2013] showed that the Antarctic continental slope suppresses mesoscale eddies, resulting in a strong sensitivity of the AABW export to the Antarctic easterly winds. However, the warm, mid-depth CDW layer is absent in these buoyancy-only simulations.

The present study is motivated by stretches of the Antarctic continental shelf over which AABW is formed and exported, particularly the western Weddell Sea [*Thompson and Heywood*, 2008]. In such regions the export of dense water onto the continental slope modifies the stratification in such a way that density surfaces, or isopycnals, directly connect the shelf waters with the CDW offshore [*Nicholls et al.*, 2009]. This isopycnal connection offers a route for CDW to cross onto the continental shelf via the action of mesoscale eddies, as illustrated in Figure 1(a). Recent glider observations capture this process in the northwest Weddell Sea [*Thompson et al.*, 2014]. In this article we test the hypothesis that these stretches of the ASF support a dynamically important shoreward eddy transport of CDW, and thus heat. We further investigate how the ASF's structure and cross-slope exchange are shaped by local conditions along various stretches of the Antarctic continental slope. We approach this problem by constructing a high resolution, eddy-resolving process model of the ASF, described in §2. In §3 we explore the sensitivity of the ASF's cross-slope transport and structure to various aspects of the surface forcing, continental slope geometry, and numerical discretization. In §4 we discuss the implications of our results and the outlook for further research.

2. An eddy-resolving model of the ASF

The configuration of our model study is strongly constrained by the requirement that mesoscale eddy motions be adequately resolved. In §3 we show that a horizontal grid spacing of 1 km or finer is needed to capture the shoreward transport of CDW. It is also important that each simulation reach statistically steady state, as otherwise the results could be strongly dependent on arbitrary choices made in setting the initial conditions [*c.f. St-Laurent et al.*, 2013]. To adequately explore the physical controls on the cross-slope transport it is also necessary to explore a wide range of simulation parameters, which multiplies the computational burden. These constraints motivate the use of an idealized model configuration in a small domain. Yet a realistic representation of the water masses is desireable for the purpose of
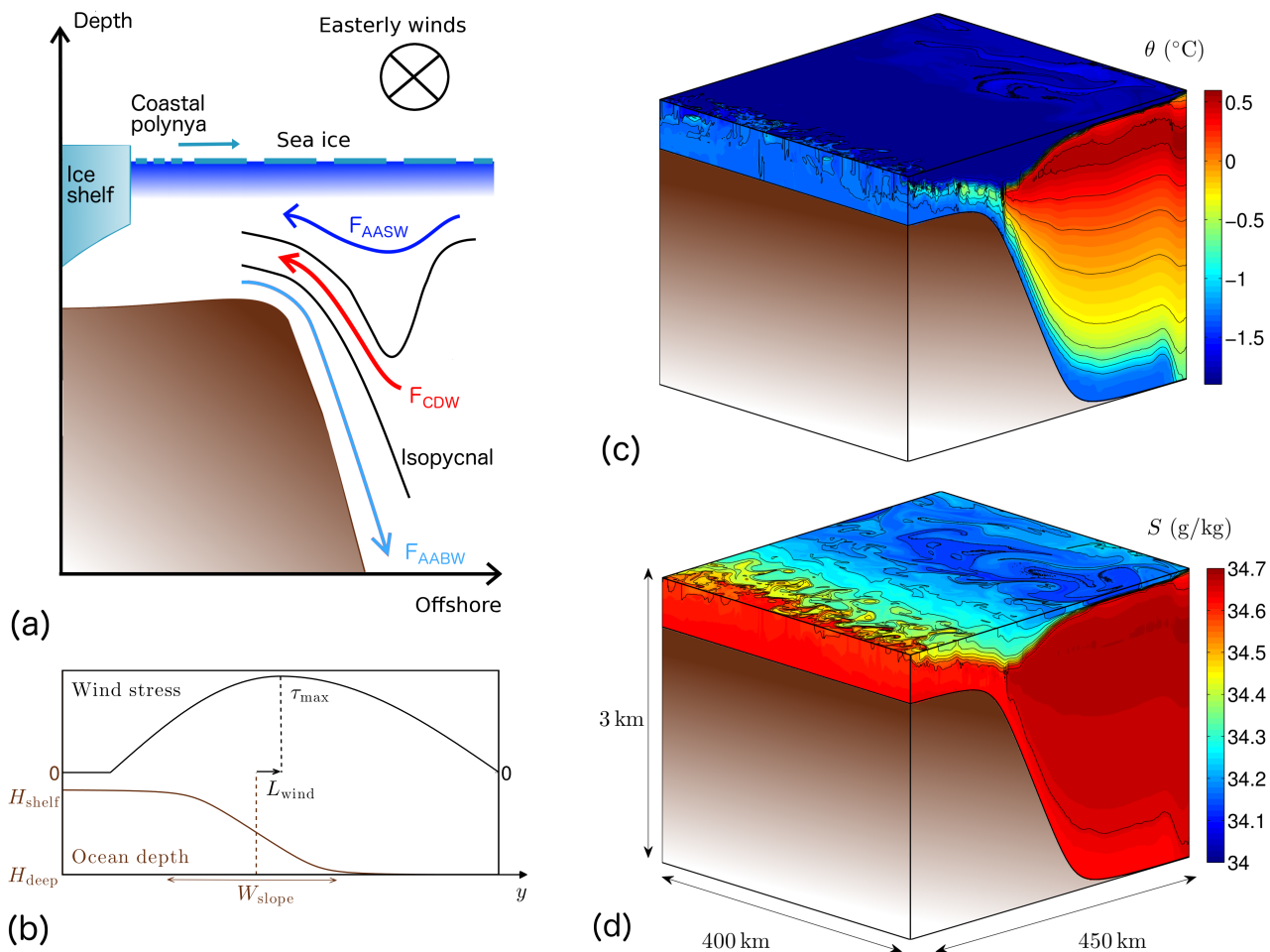
Figure 1. (a) Schematic cross-section of the Antarctic Slope Front (ASF), which separates the continental shelf waters from the warm Circumpolar Deep Water (CDW) at mid-depth offshore. In regions of Antarctic Bottom Water (AABW) outflow, such as the western Weddell and Ross Seas, isopycnal surfaces connecting the shelf waters to the CDW may facilitate onshore heat transport and AABW export via the action of mesoscale eddies. (b) Schematic profiles of ocean depth and along-shore surface wind stress used in our process model, highlighting several of the parameters varied in our sensitivity study. (c,d) Snapshots of the potential temperature and salinity in our ASF process model, described in the text. Eddy boluses of warm CDW are visible crossing the shelf break in panel (c).

comparison with the real ocean, and because it allows characterization of water mass transformation between neutral density classes [*Jackett and McDougall*, 1997]. The latter is important because in the ASF there is often no potential density that is stably stratified, due to non-linearities in the equation of state.

Our compromise between these constraints is illustrated in Figure 1(c–d), which shows an isometric view of the instantaneous potential temperature and salinity in our reference simulation. The potential temperature most clearly distinguishes the surface freshwater layer, which we refer to for simplicity as Antarctic Surface Water (AASW), from the warm, salty CDW at mid-depth and the cold, fresh AABW outflow along the ocean bed. The AASW/CDW boundary forms a characteristic 'V'-shape over the continental slope, which supports a surface-intensified slope current that flows with the shelf break to the left (see Supplementary Figure S1). Eddy stirring of the CDW onto the continental shelf is visible in the potential temperature snapshot. The salinity snapshot highlights the presence of large (50–100 km) mesoscale eddies in the deep ocean and generation of energetic submesoscale eddies over the continental shelf. The

eddies are less in evidence over the continental slope, where they are suppressed by the strong topographic vorticity gradient [*Isachsen*, 2011; *Stewart and Thompson*, 2013].

We conducted our simulations using the MIT general circulation model [MITgcm, *Marshall et al.*, 1997a, b], which we configured in a 450 km (across-slope) by 400 km (along-slope) by 3000 m (depth) re-entrant channel, as indicated in Figure 1(d). The bathymetry is symmetric in the along-shore direction, while in the across-shore direction it follows a tanh-like profile characterized by a minimum depth $H_{shelf} = 500$ m, a maximum depth $H_{deep} = 3000$ m, and a slope of width $W_{slope} = 150$ km. This profile is plotted in Figure 1(b). The slope is centered at $y = Y_{slope} = 200$ km, where y is the cross-slope Cartesian coordinate with $y = 0$ at the shoreward boundary. The domain lies on an f-plane with Coriolis parameter $f_0 = -1.31 \times 10^{-4}$ rad s^{-1}.

Away from the shoreward boundary ($y > 50$ km) we impose a steady, along-shore surface wind stress, oriented such that the continental shelf lies to the left of the winds. The wind stress has a piecewise-sinusoidal profile, vanishing at $y = 50$ km and $y = 450$ km. The wind stress maximum of $\tau_{max} = 0.075$ N m^{-2} is offset from the center of the continental slope by an offshore distance of $L_{wind} = 25$ km. This profile is plotted in Figure 1(b). To parametrize thermodynamic

Table 1. Model parameters varied in our sensitivity study. Reference values are used in our reference simulation, shown in Figure 1(c)–(d). Range indicates the variation of each parameter in our sensitivity study, with all other parameters held constant and equal to their Reference values.

Parameter	Description	Reference	Range
τ_{max}	Wind stress maximum	$0.075\,\mathrm{N\,m^{-2}}$	$0-0.1\,\mathrm{N\,m^{-2}}$
$\Sigma_{\mathrm{polynya}}$	Polynya salt input	$2.5 \times 10^{-3}\,\mathrm{g\,m^{-2}\,s^{-1}}$	$1.5-3.5 \times 10^{-3}\,\mathrm{g\,m^{-2}\,s^{-1}}$
H_{shelf}	Continental shelf depth	$500\,\mathrm{m}$	$300-700\,\mathrm{m}$
W_{slope}	Continental slope width	$150\,\mathrm{km}$	$50-250\,\mathrm{km}$
L_{wind}	Wind stress max. offset	$25\,\mathrm{km}$	$-75-125\,\mathrm{km}$
$\Delta_{\boldsymbol{x}}$	Model grid spacing	$1\,\mathrm{km}$	$0.5-10\,\mathrm{km}$

exchanges with sea ice we also impose a uniform, static, 1 m-thick layer of sea ice with a concentration of 100%. The ocean surface is then subject to surface heat and salt fluxes according to the two-equation model of *Schmidt et al.* [2004]. At the ocean bed we extract the surface-input momentum via a linear drag with coefficient $r_b = 1 \times 10^{-3}\,\mathrm{m\,s^{-1}}$.

To drive water mass transformation on the continental shelf we prescribe a uniform salt input of $\Sigma_{\mathrm{polynya}} = 2.5 \times 10^{-3}\,\mathrm{g\,m^{-2}\,s^{-1}}$ over the shoreward 50 km of the domain, crudely parametrizing brine rejection in a coastal polynya. This corresponds to sea ice formation at a rate of around $1\,\mathrm{cm\,s^{-1}}$, an order of magnitude smaller than the real Ronne polynya, but over an area that is an order of magnitude larger [*Haid and Timmermann*, 2013]. We do not impose any surface thermal forcing in this region. We found it necessary to impose this additional, explicit sink of buoyancy on the continental shelf in order to achieve a statistically-steady state in our re-entrant domain. If $\Sigma_{\mathrm{polynya}}$ is too small ($\lesssim 1.5 \times 10^{-3}\,\mathrm{g\,m^{-2}\,s^{-1}}$) then AABW is still produced by virtue of the sea ice-like thermodynamic forcing at the ocean surface, but the AABW outflow enters a spurious decadal periodic cycle in which the shelf waters are gradually densified until they can sink to the ocean bed.

At the offshore edge of the domain we restore a 50 km-wide layer to a potential temperature and salinity profile that is representative of the Weddell Sea, with a timescale of 56 days. The selected profile is based on observations from *Thompson and Heywood* [2008], but smoothed to remove small-scale noise and interpolated to remove the surface AASW layer and the deep layer of AABW: this ensures that neither the model's AASW nor its AABW are artificially imposed by the restoring. The restoring timescale varies linearly from zero at $y = 400\,\mathrm{km}$ to 56 days at $y = 450\,\mathrm{km}$. We similarly restore the velocity to zero in this region to avoid the development of a spurious jet at the northern wall, using a shorter restoring timescale of 28 days.

The horizontal grid spacing is $\Delta_{\boldsymbol{x}} = 1\,\mathrm{km}$, and there are 53 vertical grid boxes with heights ranging from 13m at the surface to 100m at the ocean bed. The numerical time step is $\Delta_t = 179\,\mathrm{s}$. Advection of temperature and salinity is performed using a second-order moment advection scheme [*Prather*, 1986] in order to minimize spurious numerical mixing [*Hill et al.*, 2012]. For numerical stability we apply a horizontal Laplacian viscosity of $12\,\mathrm{m^2\,s^{-1}}$ and a vertical Laplacian viscosity of $3 \times 10^{-4}\,\mathrm{m^2\,s^{-1}}$. We also employ a horizontal biharmonic viscosity with CFL number 0.1, and biharmonic Leith and modified-Leith viscosities [*Fox-Kemper and Menemenlis*, 2008] with coefficients both equal to 1. The only explicit mixing of potential temperature and salinity is via a vertical diffusivity of $5 \times 10^{-6}\,\mathrm{m^2\,s^{-1}}$. This mixing is supplemented by the K-Profile Parametrization [KPP, *Large et al.*, 1994], which enforces a surface mixed layer of at least 50 m depth. The ocean's equation of state is computed using the numerically efficient algorithm of *McDougall et al.* [2003].

3. Sensitivity to surface forcing and continental slope geometry

To investigate the dynamical controls on the cross-slope transports of AASW, CDW and AABW, we conduct a series of sensitivity experiments varying the wind stress maximum τ_{max}, the polynya salt forcing $\Sigma_{\mathrm{polynya}}$, the shelf depth H_{shelf}, the continental slope width W_{slope}, the wind stress offset L_{wind}, and the grid spacing $\Delta_{\boldsymbol{x}}$. These parameter variations are summarized in Table 1. In each parameter configuration we first integrate the model at 2 km horizontal resolution until the total mean energy and eddy kinetic energy (EKE) reach a statistically steady state, typically requiring around 40 years. We then interpolate the instantaneous model state onto a 1 km grid and continue the integration until the steady state is re-established, typically a further 5–20 years. We derive our results using averages over the final 5 years of model integration.

We find that the cross-slope transport can consistently be partitioned into a shoreward flux of AASW (F_{AASW}), a shoreward flux of CDW (F_{CDW}), and an offshore flux of AABW ($F_{\mathrm{AABW}} = F_{\mathrm{AASW}} + F_{\mathrm{CDW}}$), as illustrated in Figure 1. To diagnose these fluxes we first compute the model's overturning circulation streamfunction ψ, which is most accurately calculated using the fluxes within density surfaces [*Döös and Webb*, 1994; *Stewart and Thompson*, 2012]. In general there is no choice of potential density that increases monotonically with depth, whereas neutral density is stably stratified almost everywhere [*Jackett and McDougall*, 1997]. To avoid the heavy computational burden associated with computing neutral density throughout the domain at frequent time intervals, we use the Transformed Eulerian Mean (TEM) based on the locally-referenced potential density at each depth [*McIntosh and McDougall*, 1996], which closely approximates the mean isoneutral fluxes computed from the daily-averaged model output (see Supplementary Figure S2). Note that the along-shore periodicity of our model domain makes this calculation possible: it is not possible to derive a closed overturning streamfunction in a regional model due to the open boundaries.

In each case we compute F_{AABW} following *Stewart and Thompson* [2012]: we first identify all offshore-flowing streamlines that connect the shelf break ($y = 100\,\mathrm{km}$) continuously to the edge of the sponge region ($y = 400\,\mathrm{km}$). Then we define F_{AABW} as the maximum strength of overturning streamfunction ψ over all such streamlines. This excludes any streamlines that form closed loops in the interior of the domain, and therefore do not contribute to the net export of AABW. We similarly define F_{CDW} using shoreward-flowing streamlines for salinities greater than $S = 34.543\,\mathrm{g\,kg^{-1}}$, and finally calculate $F_{\mathrm{AASW}} = F_{\mathrm{AABW}} - F_{\mathrm{CDW}}$. This calculation procedure is illustrated in Supplementary Figure S2. In our reference simulation we obtain $F_{\mathrm{AASW}} = 0.20\,\mathrm{Sv}$, $F_{\mathrm{CDW}} = 0.07\,\mathrm{Sv}$ and $F_{\mathrm{AABW}} = 0.27\,\mathrm{Sv}$. Note that these transports appear small because our domain spans an along-shore distance of only 400 km.
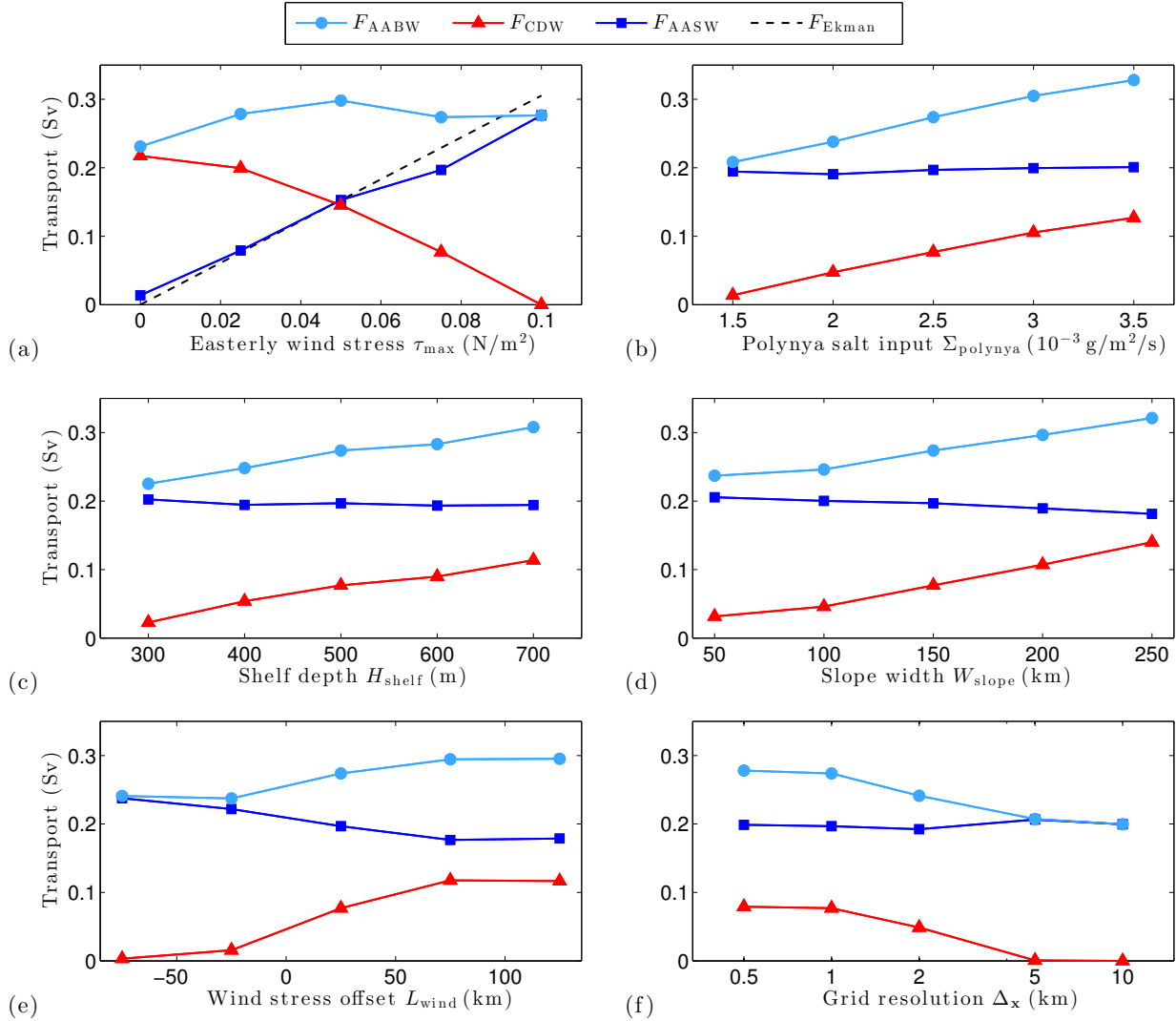
Figure 2. Cross-slope transports of Antarctic Surface Water (F_{AASW}), Circumpolar Deep Water (F_{CDW}) and Antarctic Bottom Water (F_{AABW}), which are sketched in Figure 1 and defined in §3, to surface forcing and bathymetry. The panels show the sensitivity to (a) the wind stress maximum amplitude $\tau_{\max}$, (b) the brine rejection rate on the continental shelf $\Sigma_{\mathrm{polynya}}$, (c) the depth of the continental shelf H_{shelf}, (d) the width of the continental slope W_{slope}, (e) the offset of the wind stress maximum from the center of the continental slope (L_{wind}), and (f) the model's horizontal grid spacing $\Delta_{\boldsymbol{x}}$. Panel (a) also shows the theoretical wind-driven southward surface Ekman transport ($F_{\mathrm{Ekman}} = \tau_{\max}/\rho_0|f_0|$), which agrees closely with the shoreward transport of AASW.

The shoreward transport of AASW varies almost linearly with the wind stress maximum $\tau_{\max}$, but is insensitive to all of the other model parameters varied in this study. In Figure 2(a) we demonstrate that F_{AASW} is closely predicted by the theoretical maximum shoreward wind-driven Ekman transport, $F_{\mathrm{Ekman}} = \tau_{\max}/\rho_0|f_0|$. This indicates that the shoreward AASW transport is wind-driven, with diabatic transformations in the surface layer supported by heat and salt exchanges with the sea ice. Our re-entrant domain cannot support a geostrophic shoreward transport, so the shoreward flux of CDW in the ocean interior is accomplished by mesoscale eddy transport [*c.f. Marshall and Radko*, 2003]. An interior shoreward mean flow can also be supported by eddy momentum flux divergence [*e.g. Spall*, 2013], but this mechanism makes a negligible contribution to the cross-slope transport in our model. Figure 2(a) shows that F_{CDW} decreases almost linearly with $\tau_{\max}$, in such a way that the AABW export F_{AABW} remains approximately unchanged, varying by around 20% over the range of wind

stresses considered here. By contrast, in panels (b)–(f) the AABW export is sensitive to all other aspects of the model forcing, geometry and discretization, and that this sensitivity is almost entirely due to changes in the shoreward CDW transport F_{CDW}; the shoreward AASW transport is essentially fixed by $\tau_{\max}$. Remarkably, varying any one of the six parameters selected for this sensitivity study can shift the ASF from a regime in which almost no CDW crosses the shelf break to one in which F_{CDW} is comparable to F_{AASW}.

The sensitivity of F_{CDW} to each individual parameter may be understood as follows. Increasing $\tau_{\max}$ steepens the isopycnals in the ASF, deepening the pycnocline at the shelf break until CDW can no longer mix across it (see Figure 3). Increasing $\Sigma_{\mathrm{polynya}}$ increases the input of available potential energy on the continental shelf, which is partly released as EKE on the continental shelf and slope, enhancing the rate of eddy CDW transport. Note that the isopycnals close to the ocean bed over the continental slope are shoaled to
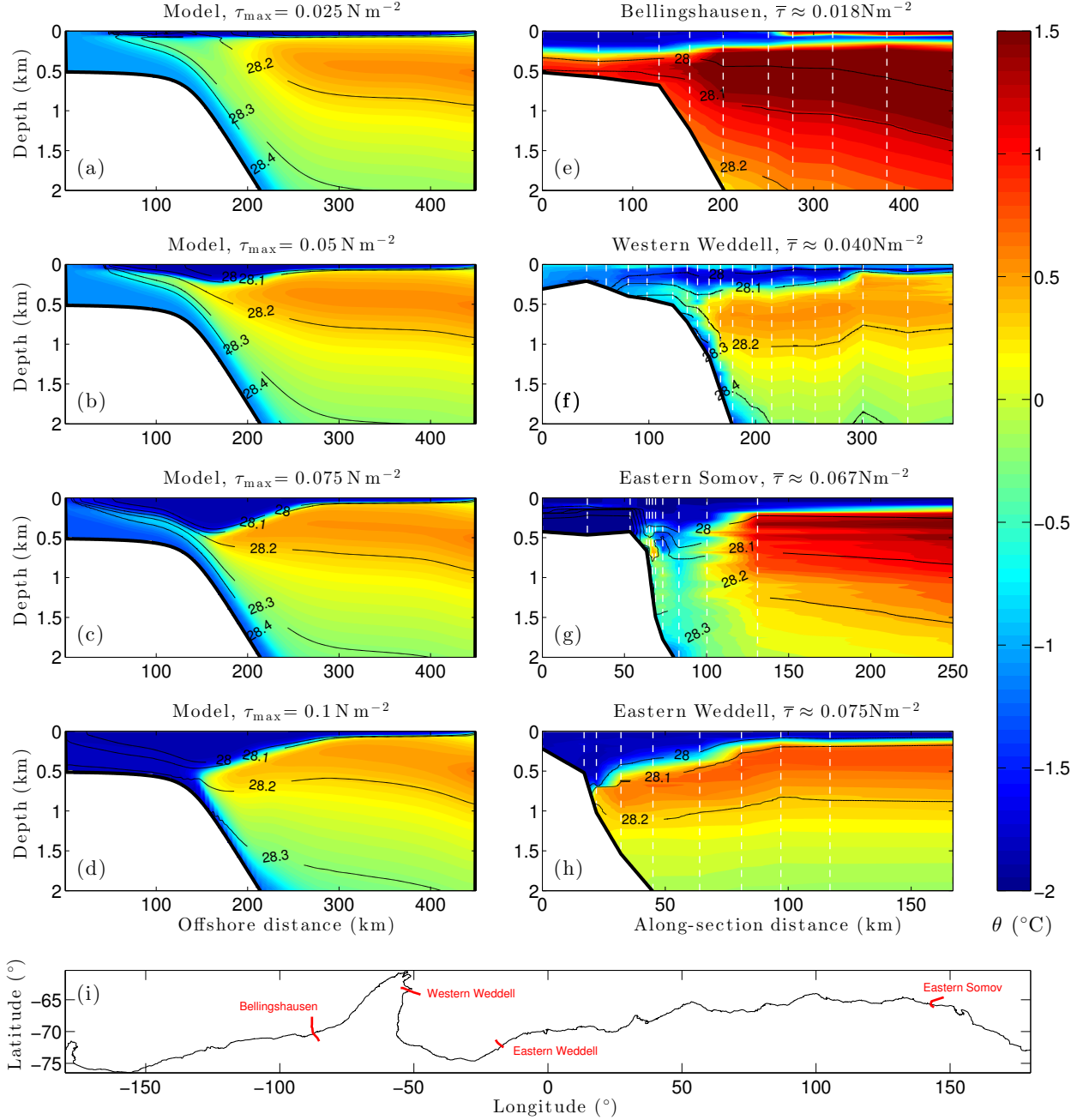
Figure 3. Comparison between simulated and observed potential temperature (colors) and neutral density (black contours). (a–d) Time- and along-shore-mean properties in our process model for a range of surface wind stress maxima. (e–h) Cross-slope hydrographic sections from, the eastern Somov Sea [*Gordon et al.*, 2004], the western Weddell Sea [*Thompson and Heywood*, 2008], the Bellingshausen Sea and the eastern Weddell Sea [*Orsi and Whitworth*, 2005]. Vertical white dashed lines indicate cast locations. (i) Map of the 1000 m depth contour around Antarctica (black) [*Amante and Eakins*, 2009] with selected hydrographic sections (red). For each section we estimated the local wind stress $\overline{\tau}$ directed along the 1000 m depth contour from the CORE.v2 dataset [*Large and Yeager*, 2009].

the south (see Figure. 3), so both the surface wind stress and mesoscale eddies serve to extract available potential energy (APE), and thus the APE must be sourced from $\Sigma_{\mathrm{polynya}}$. Increasing H_{shelf} deepens the continental shelf, allowing more CDW isopycnals to connect with the shelf waters. Increasing W_{slope} reduces the topographic potential vorticity gradient, allowing the slope to support larger eddies that transport CDW shoreward more rapidly. Shifting the

surface wind stress maximum simply changes the effective wind stress over the continental slope, which in turn modifies F_{CDW} by changing the pycnocline depth at the shelf break. Finally, reducing the numerical grid spacing Δ_x resolves baroclinic instabilities at shorter wavelengths, which increases the conversion of potential energy to EKE on the continental slope, and thus enhances the eddy transport of CDW. We find that there is no further increase in F_{CDW} for $\Delta_x \leq 1$ km because at this point the model resolves the first

Rossby radius of deformation, which is around 4 km on the continental slope.

Of all of the parameters examined in this study, the ASF's structure and transport are particularly sensitive to the along-slope wind stress. Our simulations suggest that much of the regional variation in the structure of the ASF can be explained by the local along-shore winds. To illustrate this idea, in Figure 3(a)–(d) we plot the simulated time- and along-shore-mean potential temperature and neutral density obtained for increasing wind strengths $\tau_{\max}$, with all other aspects of the model configuration held fixed. Panels (e)–(h) show hydrographic sections from the Bellingshausen, Somov and Weddell Seas that are subject to comparable mean wind stress along the 1000 m depth contour [*Amante and Eakins*, 2009]. In each case we computed the average along-slope wind stress along a $\sim$ 300 km stretch of the 1000 m depth contour, using the CORE.v2 surface wind stress data [*Large and Yeager*, 2009] averaged between 1996 and 2006. Note that this dataset does not account for sea ice, which can enhance the ocean surface wind stress by up to 50% [*e.g. Fujisaki et al.*, 2010]. Our idealized model has not been tailored to simulate these sections of the ocean, and consequently there are several clear differences between the simulations and the observations, most obviously the presence of AABW in panels (a) and (d). The agreement is arguably worst for the Bellingshausen (panels (a) and (e)), where the overturning circulation is fundamentally different, with a warm inflow along the ocean bed on the continental shelf and surface outflow of fresh water from the ice shelves [*e.g. Potter et al.*, 1988]. However, the striking qualitative agreement in the isopycnal structure over the continental slope and the penetration of CDW onto the continental shelf suggests that the local along-shore wind stress controls the pycnocline depth at the shelf break, and thereby limits the eddy-driven shoreward CDW transport.

4. Discussion

This study elucidates the dependence of the ASF's structure and cross-slope transport on various aspects of the local surface forcing and continental shelf geometry. If we regard our model as a conceptual representation of the mean cross-slope exchanges around the entire $\sim$ 20,000 km length of Antarctica's 1000 m depth contour [*Amante and Eakins*, 2009], then our reference simulation predicts a total shoreward CDW transport of around 3.5 Sv. Using a typical CDW potential temperature of 0°C over the continental slope, we estimate that this corresponds to a shoreward heat transport, relative to the surface freezing temperature of $\sim$ −1.8°C, of around 25 TW. Though this estimate is over-simplified, it supports the hypothesis that mesoscale eddies transfer CDW across the Antarctic shelf break at a dynamically significant rate. A comparable calculation for the AASW yields a shoreward transport of around 10 Sv, but essentially zero heat transport because this layer is so close to the freezing temperature. Note that in the real ocean, surface warming during the austral summer does produce a wind-driven shoreward heat transport in the AASW layer [*Zhou et al.*, 2014].

A distinguishing feature of our model is that it fully resolves mesoscale eddies, as demonstrated by Figure 2(f), and achieves a statistically steady state in all simulations. Comparable previous studies of the Antarctic shelf break have configured eddy-resolving models as initial-value problems [*e.g. Nøst et al.*, 2011; *St-Laurent et al.*, 2013; *Nakayama et al.*, 2014; *Zhou et al.*, 2014], which may introduce an arbitrary dependence on the models' initial conditions. However, it was necessary to idealize certain aspects of our simulations, and our results should be interpreted with these limitations in mind. In particular we omit lateral variations, such as canyons and ridges, that can support mean geostrophic flows onto the continental shelf [*Nicholls et al.*, 2009]. Our treatments of the surface wind stress, ocean-sea ice interaction, and dense water production on the continental shelf are simplistic, and omit any representation of the coastal ocean's pronounced seasonal cycle [*Jacobs*, 2004]. As a result our model cannot represent the role of Antarctic gyre circulations and the Antarctic Circumpolar Current in shaping the ASF, relying solely on local surface wind forcing. Importantly, we have also neglected the influence of tidal mixing and transport, which is particularly pronounced on continental slopes and has been shown to induce a substantial shoreward transport of CDW in the western Ross Sea [*Wang et al.*, 2013]. Despite these shortcomings, our model qualitatively captures the structure of the real ASF in various regions (see Figure 3).

A key result of our sensitivity study is that the ASF's cross-slope transport can be partitioned into a purely wind-driven shoreward transport of surface waters (F_{AASW} in Figure 1), an interior eddy transport of CDW (F_{CDW}), and an export of AABW along the ocean bed (F_{AABW}). The eddy-driven shoreward transport of CDW is sensitive to all aspects of the model's forcing, geometry, and grid resolution considered in this study. Changing any one of the wind stress maximum, salt input on the continental shelf, continental shelf depth, continental slope width, or wind stress position can essentially shut off the shoreward transport of CDW. Given that these parameters vary substantially around the Antarctic margins, it is likely that the shoreward eddy transport of CDW is localized to favorable sections of the continental slope. The dependence of F_{CDW} on each of the model parameters is physically intuitive, as set out in §3. However, these arguments do not satisfactorily explain the response of the eddy kinetic energy over the slope (not shown), which is closely related to the rate of eddy transfer of mass and tracers [*e.g. Ferrari and Nikurashin*, 2010]. To understand this comprehensively requires a careful analysis of the energetics over the continental slope; this is the subject of ongoing work.

We emphasize that the eddy transport of CDW is completely absent even at a numerical grid spacing as fine as 5 km, and is underestimated by close to 50% even at 2 km resolution. *St-Laurent et al.* [2013] similarly found that a 1 km horizontal resolution was required to adequately resolve eddies on the continental shelf. This corresponds to a longitudinal resolution of around $1/48°$, which would incur an excessive computational cost in any global ocean model; even the Southern Ocean State Estimate (SOSE) uses only $1/6°$ resolution [*Mazloff et al.*, 2010]. In models coarser than this $1/48°$ cutoff, the cross-slope eddy transfer coefficient must be parametrized carefully to ensure that the shelf water masses are accurately represented [*Stewart and Thompson*, 2013].

Our model's sensitivity to the along-shore wind stress, shown in Figure 2(a), and the qualitative agreement between the observed and modeled ASF structure at various wind strengths, shown in Figure 3, suggest that the Antarctic easterlies exert substantial influence over transport and mixing across the continental shelf break [*c.f. Stewart and Thompson*, 2012]. This implies that past and future changes in the along-shore winds could substantially alter the exchanges of mass, heat, salt, and biogeochemical tracers across the Antarctic shelf break, with potentially dramatic implications for the ocean's abyssal circulation, ventilation and carbon storage [*Jacobs*, 2004]. Consistent with our findings, *Spence et al.* [2014] have shown that a southward shift of the mid-latitude westerlies, weakening the Antarctic easterlies, warms the Antarctic subsurface coastal waters by up to 2°C due to weakening of the shoreward surface Ekman transport. Further work is required to quantify the contribution of the along-shore winds to the variety of ASF structures observed around the Antarctic margins.

References

Amante, C., and B. W. Eakins, ETOPO1 1 Arc-Minute Global Relief Model: Procedures, Data Sources and Analysis., *Tech. Rep. NESDIS NGDC-24*, NOAA, 2009.

Döös, K., and D. J. Webb, The Deacon cell and the other meridional cells of the Southern Ocean, *J. Phys. Oceanogr.*, *24*, 429–429, 1994.

Ferrari, R., and M. Nikurashin, Suppression of eddy diffusivity across jets in the Southern Ocean, *J. Phys. Oceanogr.*, *40*(7), 1501–1519, 2010.

Fox-Kemper, B., and D. Menemenlis, Can large eddy simulation techniques improve mesoscale rich ocean models?, *Geophys. Monogr. Ser.*, *177*, 319–338, 2008.

Fujisaki, A., H. Yamaguchi, and H. Mitsudera, Numerical experiments of air–ice drag coefficient and its impact on ice–ocean coupled system in the Sea of Okhotsk, *Ocean Dyn.*, *60*(2), 377–394, 2010.

Gebbie, G. A., and P. Huybers, How is the ocean filled?, *Geophys. Res. Lett.*, *38*, 2011.

Gordon, A. L., E. Zambianchi, A. Orsi, M. Visbeck, C. F. Giulivi, T. Whitworth, and G. Spezie, Energetic plumes over the western Ross Sea continental slope, *Geophys. Res. Lett.*, *31*(21), 2004.

Haid, V., and R. Timmermann, Simulated heat flux and sea ice production at coastal polynyas in the southwestern Weddell Sea, *J. Geophs. Res.*, *118*(5), 2640–2652, 2013.

Hattermann, T., L. H. Smedsrud, O. A. Nøst, J. M. Lilly, and B. K. Galton-Fenzi, Eddy-resolving simulations of the Fimbul Ice Shelf cavity circulation: Basal melting and exchange with open ocean, *Ocean Modell.*, *82*, 28–44, 2014.

Hill, C., D. Ferreira, J.-M. Campin, J. Marshall, R. Abernathey, and N. Barrier, Controlling spurious diapycnal mixing in eddy-resolving height-coordinate ocean models–Insights from virtual deliberate tracer release experiments, *Ocean Modell.*, *45*, 14–26, 2012.

Isachsen, P. E., Baroclinic instability and eddy tracer transport across sloping bottom topography: How well does a modified Eady model do in primitive equation simulations?, *Ocean Modell.*, *39*(1), 183–199, 2011.

Jackett, D. R., and T. J. McDougall, A neutral density variable for the world's oceans, *J. Phys. Oceanogr.*, *27*(2), 237–263, 1997.

Jacobs, S. S., On the nature and significance of the Antarctic Slope Front, *Mar. Chem.*, *35*(1), 9–24, 1991.

Jacobs, S. S., Bottom water production and its links with the thermohaline circulation, *Antarct. Sci.*, *16*(04), 427–437, 2004.

Jacobs, S. S., A. Jenkins, C. F. Giulivi, and P. Dutrieux, Stronger ocean circulation and increased melting under Pine Island Glacier ice shelf, *Nat. Geosci.*, *4*(8), 519–523, 2011.

Large, W. G., and S. G. Yeager, The global climatology of an interannually varying air–sea flux data set, *Climate Dynam.*, *33*(2), 341–364, 2009.

Large, W. G., J. C. McWilliams, and S. C. Doney, Oceanic vertical mixing: A review and a model with a nonlocal boundary layer parameterization, *Rev. Geophys.*, *32*(4), 363–404, 1994.

Lumpkin, R., and K. Speer, Global ocean meridional overturning, *J. Phys. Oceanogr.*, *37*(10), 2550–2562, 2007.

Marshall, J., and T. Radko, Residual-mean solutions for the Antarctic Circumpolar Current and its associated overturning circulation, *J. Phys. Oceanogr.*, *33*(11), 2341–2354, 2003.

Marshall, J., A. Adcroft, C. Hill, L. Perelman, and C. Heisey, A finite-volume, incompressible Navier Stokes model for studies of the ocean on parallel computers, *J. Geophys. Res.*, *102*, 5753–5766, 1997a.

Marshall, J., C. Hill, L. Perelman, and A. Adcroft, Hydrostatic, quasi-hydrostatic, and nonhydrostatic ocean modeling, *J. Geophys. Res.*, *102*, 5733–5752, 1997b.

Mazloff, M. R., P. Heimbach, and C. Wunsch, An eddy-permitting Southern Ocean state estimate, *J. Phys. Oceanogr.*, *40*(5), 880–899, 2010.

McDougall, T. J., D. R. Jackett, D. G. Wright, and R. Feistel, Accurate and computationally efficient algorithms for potential temperature and density of seawater, *J. Atmos. Oceanic Technol.*, *20*(5), 730–741, 2003.

McIntosh, P. C., and T. J. McDougall, Isopycnal averaging and the residual mean circulation, *J. Phys. Oceanogr.*, *26*(8), 1655–1660, 1996.

Nakayama, Y., K. I. Ohshima, Y. Matsumura, Y. Fukamachi, and H. Hasumi, A Numerical Investigation of Formation and Variability of Antarctic Bottom Water off Cape Darnley, East Antarctica, *J. Phys. Oceanogr.*, *44*(11), 2921–2937, 2014.

Nicholls, K. W., S. Østerhus, K. Makinson, T. Gammelsrød, and E. Fahrbach, Ice-ocean processes over the continental shelf of the southern Weddell Sea, Antarctica: A review, *Rev. Geophys.*, *47*(3), 2009.

Nøst, O. A., M. Biuw, V. Tverberg, C. Lydersen, T. Hattermann, Q. Zhou, L. H. Smedsrud, and K. M. Kovacs, Eddy overturning of the Antarctic Slope Front controls glacial melting in the Eastern Weddell Sea, *J. Geophys. Res*, *116*, C11,014, 2011.

Orsi, A. H., and T. Whitworth, *Hydrographic Atlas of the World Ocean Circulation Experiment (WOCE): Volume 1: Southern Ocean*, WOCE International Project Office, 2005.

Orsi, A. H., G. C. Johnson, and J. L. Bullister, Circulation, mixing, and production of Antarctic Bottom Water, *Prog. Oceanogr.*, *43*(1), 55–109, 1999.

Orsi, A. H., S. S. Jacobs, A. L. Gordon, and M. Visbeck, Cooling and ventilating the abyssal ocean, *Geophys. Res. Lett.*, *28*(15), 2923–2926, 2001.

Potter, J. R., M. H. Talbot, and J. G. Paren, Oceanic regimes at the ice fronts of George VI Sound, Antarctic Peninsula, *Cont. Shelf Res.*, *8*(4), 347–362, 1988.

Prather, M. J., Numerical advection by conservation of second-order moments, *J. Geophys. Res.*, *91*(D6), 6671–6681, 1986.

Schmidt, G. A., C. M. Bitz, U. Mikolajewicz, and L.-B. Tremblay, Ice–ocean boundary conditions for coupled models, *Ocean Modell.*, *7*(1), 59–74, 2004.

Schmidtko, S., K. J. Heywood, A. F. Thompson, and S. Aoki, Multidecadal warming of Antarctic waters, *Science*, *346*(6214), 1227–1231, 2014.

Skinner, L., S. Fallon, C. Waelbroeck, E. Michel, and S. Barker, Ventilation of the deep Southern Ocean and deglacial CO2 rise, *Science*, *328*(5982), 1147–1151, 2010.

Spall, M. A., Dense water formation around islands, *J. Geophys. Res.: Oceans*, *118*(5), 2507–2519, 2013.

Spence, P., S. M. Griffies, M. H. England, A. M. Hogg, O. A. Saenko, and N. C. Jourdain, Rapid subsurface warming and circulation changes of Antarctic coastal waters by poleward shifting winds, *Geophys. Res. Lett.*, *41*(13), 4601–4610, 2014.

St-Laurent, P., J. M. Klinck, and M. S. Dinniman, On the role of coastal troughs in the circulation of warm circumpolar deep water on Antarctic shelves, *J. Phys. Oceanogr.*, *43*(1), 51–64, 2013.

Stewart, A. L., and A. F. Thompson, Sensitivity of the ocean's deep overturning circulation to easterly Antarctic winds, *Geophys. Res. Lett.*, *39*(18), L18,604, 2012.

Stewart, A. L., and A. F. Thompson, Connecting Antarctic Cross-Slope Exchange with Southern Ocean Overturning, *J. Phys. Oceanogr.*, *43*, 1453–1471, 2013.

Thompson, A. F., and K. J. Heywood, Frontal structure and transport in the northwestern Weddell Sea, *Deep-Sea Res. Pt. I*, *55*(10), 1229–1251, 2008.

Thompson, A. F., K. J. Heywood, S. Schmidtko, and A. L. Stewart, Eddy transport as a key component of the Antarctic overturning circulation, *Nat. Geosci.*, *7*(12), 879–884, 2014.

Wang, Q., S. Danilov, H. Hellmer, D. Sidorenko, J. Schroeter, and T. Jung, Enhanced cross-shelf exchange by tides in the western Ross Sea, *Geophys, Res. Lett.*, *40*(21), 5735–5739, 2013.

Zhou, Q., T. Hattermann, O. A. Nøst, M. Biuw, K. M. Kovacs, and C. Lydersen, Wind-driven spreading of fresh surface water beneath ice shelves in the Eastern Weddell Sea, *J. Geophys. Res.*, *119*, 3818–3833, 2014.

A. L. Stewart, Department of Atmospheric and Oceanic Sciences, University of California, Los Angeles, Los Angeles, CA 90095, USA. (astewart@atmos.ucla.edu)

A. F. Thompson, Environmental Sciences and Engineering, Linde + Robinson Laboratory, California Institute of Technology, Pasadena, CA 91125, USA. (andrewt@caltech.edu)